T H E U N I V E R S I T Y O F M I C H I G A N

COLLEGE OF ENGINEERING
Department of Aeronautical and Astronautical Engineering
Aerodynamics Laboratory

Technical Report

MEASUREMENTS OF THE FLUCTUATING PRESSURE AT THE WALL BENEATH A THICK TURBULENT BOUNDARY LAYER

W. W. Willmarth
C. E. Wooldridge

ORA Project 02920

under contract with:

DEPARTMENT OF THE NAVY
OFFICE OF NAVAL RESEARCH
CONTRACT NO. Nonr-1224(30)
WASHINGTON, D. C.

administered through:

OFFICE OF RESEARCH ADMINISTRATION ANN ARBOR

April 1962

TABLE OF CONTENTS

SUMMARY

Measurements of the turbulent pressure field at the wall beneath a thick (5-inch) turbulent boundary layer produced by natural transition on a smooth surface are reported. The data include the mean-square-pressure, power spectrum of the pressure, space-time correlation of the pressure parallel to the stream, and spatial correlation of the pressure transverse to the stream.

The root-mean-square wall pressure was 2.19 times the wall shear stress. The power spectra of the pressure were found to scale with the free-stream speed and the boundary-layer-displacement thickness. A few tests with a rough surface showed that the increase in root-mean-square wall pressure was greater than the increase in wall shear stress.

The space-time correlation measurements parallel to the stream direction exhibit maxima at certain time delays corresponding to the convection of pressure-producing eddies at speeds varying from 0.56 to 0.83 times the stream speed. The lower convection speeds are measured when the spatial separation of the pressure transducers is small or when only the pressure fluctuations at high frequencies are correlated. Higher convection speeds are observed when the spatial separation of the pressure transducers is large or when only low frequencies are correlated. The result that low-frequency pressure fluctuations have the highest convection speed is in agreement with the measurements of Corcos (1959, 1962) in a fully turbulent tube flow. Analysis of these measurements also shows that both large- and small-scale pressure-producing eddies decay after traveling a distance proportional to their scale. More

precisely, a pressure-producing eddy of large or small wave length, λ., decays and vanishes after traveling a distance of approximately 6λ.

The transverse spatial correlation of the wall-pressure fluctuations was measured and compared with the longitudinal scale. Both the transverse and the longitudinal scale of the pressure fluctuations were of the order of the boundary-layer-displacement thickness. The transverse and longitudinal scales of both large- and small-scale wall-pressure fluctuations were also measured and were also found to be approximately the same.

1. INTRODUCTION

Knowledge of the pressure fluctuations within a turbulent boundary layer is desired for many problems in fluid mechanics. One of these is the aerodynamic noise produced by turbulence in the boundary layer adjacent to a rigid surface. Another type of problem arises when a turbulent boundary layer is developed adjacent to a flexible surface, and the pressure fluctuations can cause motion of the surface normal to itself. The questions of wave generation on liquid surfaces, sound generation by motion of thin membranes or plates, and turbulence inhibition by surface motion are then of interest. In addition, knowledge of the turbulent pressure fluctuations may lead to a better understanding of the structure of the turbulent boundary layer.

The first theoretical and experimental studies of turbulent pressure fluctuations were concerned with isotropic turbulence. The papers of Batchelor (1950) and Uberoi (1953) represent relatively recent contributions to the theoretical and experimental literature and give historical reviews of the problem. In the boundary layer one is faced with the much more difficult problem of pressure fluctuations in anisotropic turbulence developed along a wall. Kraichman (1956a, 1956b) has shown that the primary contribution to the pressure fluctuations in the boundary layer near the wall must be attributed to the interaction of the turbulence with the mean shear. He estimated (1956b) that the magnitude of the root-mean-square pressure fluctuations at the wall were of the order of the wall shear stress. Confirmation of this estimate and additional information about the wall pressure fluctuations must be obtained

experimentally.

Direct measurements of pressure fluctuations within a turbulent flow are not possible because a suitable pressure transducer, free from interaction with the turbulent flow, does not exist. Uberoi (1953) avoided the problem of direct pressure measurement because hot-wire measurements of a certain few velocity correlations, in isotropic turbulence, can be used to compute pressure correlations. In the work reported here, the pressure fluctuations on the wall beneath the turbulent boundary layer were measured directly with a pressure transducer flush with the surface.

Experimental measurements of the wall-pressure fluctuations beneath various turbulent shear flows have already been reported: beneath turbulent boundary layers, by Harrison (1958), Willmarth (1958a, 1959), and Bull (1960) at subsonic speeds and by Kistler* at both subsonic and supersonic speeds; in a fully developed turbulent flow in a tube, by Corcos (1962); and beneath a wall jet, by Lilley and Hodgson (1960). All investigators report measurements of the spectrum of the pressure and the space-time correlation of the pressure. The correlation measurements show that the pressure fluctuations are convected downstream at approximately 0.8 U_∞ and decay after traveling a few boundary-layer thicknesses.

Very little additional information exists about the fine structure of the wall-pressure fluctuations, primarily because the previous investigations were made with pressure transducers that, compared to the boundary-layer thickness, were relatively large. The present experiments beneath a thick turbulent

*Portions of Kistler's results have been reported by Laufer (1961)

boundary layer were devised in an attempt to increase the precision of the existing experimental information and to learn more about the detailed structure of the wall-pressure fluctuations. We are also investigating the correlation between the wall pressure and the velocity components in the boundary layer to learn more about the structure and scale of the eddies that produce the pressure fluctuations. The pressure-velocity correlation measurements will be reported in a later paper.

2. EXPERIMENTAL PROCEDURE

2.1. Experimental equipment

The measurements were made on the floor of the 5- x 7-foot test section of The University of Michigan's subsonic wind tunnel. The wind-tunnel test section is 25 feet long and is indoors. The settling chamber, fan, and steel ducting that recirculates the air are out of doors. The total distance around the wind-tunnel circuit is 332 feet. The contraction ratio of the nozzle is 15:1.

The pressure measurements were made on the surface of a smooth (oil-lapped) steel disk, 1-inch thick and 20 inches in diameter, that was sealed against air leaks and inset flush with the test section's floor. Holes were drilled through the disk to allow insertion of pressure transducers or of dummy transducers (brass plugs). The plugs and transducers were always flush with the surface within ± 0.001-in. A special test established that ± 0.001-in. misalignment produced less than 1% increase in the root-mean-square wall pressure. The steel disk was welded to a hollow steel tube that was filled with

sand and fitted with legs and alignment jacks. This massive, 800-lb assembly was partially isolated from the vibrations of the concrete floor of the laboratory by thick rubber pads. Figure 1 is a sketch of the plate mounted in the wind-tunnel floor.

The fluctuating wall pressure was detected by lead zirconate pressure transducers. The transducer dimensions and construction were identical with those of the barium titanate transducers already developed and reported by Willmarth (1958b). The diameter of the sensitive area of the transducer was 0.163 in. The frequency response of the transducers was uniform in the frequency range of interest, 20 to 10,000 cps. The pressure-transducer sensitivity was determined by placing the transducers in a closed volume and varying the volume with a piston driven by a connecting rod and crankshaft. Assuming an isentropic compression or expansion, the pressure change was computed from the known volume change.

Pressure fluctuations whose scale is of the order of the diameter of the sensitive area of the transducer will not suffer appreciable attenuation. The ratio of transducer diameter, 0.163 in., to boundary-layer thickness, 5 in., was approximately 1:30. Thus we may expect that pressure fluctuations whose scale is greater than 1/30th of the boundary-layer thickness will not be attenuated by the transducer.

The voltage developed at the pressure transducer was detected by a high-impedance cathode follower and a low-noise amplifier with a maximum gain of 10^5. Figure 2 is a circuit diagram for the input stage of the amplifier. The input impedance of the cathode follower is 1.2×10^8 ohms and the gain of the

pre-amplifier is approximately 50. The root-mean-square noise level referred to the input with the transducer connected to the cathode follower is approximately 5 μvolts for a frequency band from 20 to 20,000 cps. The bulk of the noise occurs at low frequencies and can be attributed to fluctuations in the cathode follower grid current which develops quite large voltage fluctuations across the capacitive impedance of the lead zirconate pressure transducer. To reduce the fluctuations in grid current, dirt and moisture must be kept from the input circuitry and transducer. When the transducers were not being used and the air humidity was high, it was necessary to store the input circuitry and transducer in an air-tight box containing a drying agent.

The electrical signals from the pressure transducers were recorded on separate channels of a magnetic tape using an Ampex FR 1100 tape recorder. The tape recorder was fitted with a specially designed playback head assembly that allowed one signal to be time-delayed with respect to the other. The correlation of pressure signals was measured by a thermocouple that was first fed with the sum and then with the difference of the time-delayed signals from the tape recorder. The thermocouple response was detected by a Sensitive Research Corp. model SEW 5 millivoltmeter. The correlation between two signals was obtained by subtracting the thermocouple response to the difference between two signals from the response to the sum of the signals. Provisions were made to allow the sum and difference signals to be filtered by a Kronhite Model 310-AB variable band pass filter just before they entered the thermocouple.

Measurements of the spectrum of the pressure were made by passing the

signal through a General Radio type 736-A wave analyzer whose output was fed to the thermocouple. Root-mean-square measurements were made with a Ballantine Model 320 true RMS meter. Electrical signals were monitored with a DuMont Model 322-A Dual beam oscilloscope.

2.2. Coordinate system and nomenclature

A cartesian coordinate system is chosen to describe the measurements. The x and z axes lie in the plane of the wall with x increasing in the stream direction. The y axis is normal to the wall and increases as one moves away from the wall into the fluid in the boundary layer.

A number of other symbols are used to describe the measurements. The nomenclature is:

$E(\omega)$	Power spectrum of the wall pressure; see equation (3).
f	Frequency.
$F(x_1,x_3,\omega)$	Temporal Fourier transform of the normalized wall pressure correlation; see equation (4).
k	Wave number; $k = \frac{2\pi}{\lambda}$.
p	Pressure
q	Dynamic pressure
R	Reynolds number based on distance from virtual origin of turbulent boundary layer.
R_{pp}	Normalized wall pressure correlation; see equations (1) and (4)
R'_{pp}	Normalized wall pressure correlation in a frequency band; see equation (9)
τ	Time delay
τ_w	Wall shear stress

U	Mean velocity in the stream direction
U_τ	Friction velocity; $U_\tau = \sqrt{\tau_w/\rho}$
$\Delta U/U_\tau$	Displacement of boundary-layer logarithmic mean velocity profile produced by surface roughness
x_1, x_3	Spatial separation of pressure transducers in the x or z direction
δ	Boundary-layer thickness
λ	Wave length
ρ	Density
ω	Circular frequency; $\omega = 2\pi f$
$\overline{(\ )}$	Average

The subscript, ∞, refers to free-stream conditions.

3. EXPERIMENTAL ENVIRONMENT

The accuracy or validity of the experiments can be affected by the vibration of the pressure transducer, the sound field and turbulence in the flow, and the state or nature of the turbulent boundary layer. The various factors affecting the experimental environment will be discussed separately. The discussion refers, unless otherwise stated, to the highest available wind-tunnel speed, 200 ft/sec, because disturbing factors were the largest at high speeds.

3.1. Vibration of the pressure transducer

Very effective vibration isolation of the pressure transducers was obtained with the sand-filled tubular steel mounting described in section 2. The effectiveness of the mounting was tested by shielding the transducer from

the wall-pressure fluctuations while the tunnel was running. It was found that the signals caused by vibration amounted to less than 1/100 of the mean-square turbulent wall-pressure fluctuations.

3.2. Sound field in the test section

Before the wall-pressure measurements were made, the sound-pressure level and spectrum of the sound field in the settling chamber were measured in a frequency band of from 25 to 7,500 cps, with a General Radio sound level meter and sound analyzer. The spectral density of the sound had a peak at 135 cps, and otherwise was approximately proportional to the inverse square of the frequency. The mean-square sound pressure was 1/32 of the mean-square wall-pressure fluctuations that were measured later.

The sound-pressure level in the settling chamber may not accurately represent the sound-pressure level in the test section. To measure the test-section sound directly, a pressure transducer was installed flush with the surface and on the stagnation line of a streamlined model shaped like a wing tip that was exposed to the airflow in the test section.

The mean-square stagnation-pressure fluctuations were found to be approximately 1/16 of the mean-square wall-pressure fluctuations over a frequency band extending from 105 to 20,000 cps. Examination of the spectra of the stagnation-pressure fluctuations revealed peaks of the energy density at 135 and 200 cps. The peak at 135 cps corresponds to the sound produced by the wind-tunnel fan. The peak at 200 cps was not present in the settling chamber sound. The settling-chamber-sound spectrum was measured about 1-1/2 years before the stagnation-point pressure spectrum, and it is possible that the additional sound may be

caused by changes in the structural vibration of the tunnel, test section, or fan section. At frequencies above 200 cps, the stagnation-point pressure spectrum decreased approximately linearly with frequency. However, the energy density varied from day to day and even while the spectrum was being measured. We do not believe that the spectral measurements above 200 cps give a reliable estimate of the sound field in the test section. At times the streamlined model itself would rattle and produce measurable contributions to the spectra above 200 cps.

A more precise way to estimate the sound field in the test section was discovered later in the investigation. During the measurements of the longitudinal space-time correlation of the wall pressure, it was discovered that a small peak in the correlation occurred for negative time delay. The location of the peak corresponded to the speed of sound in the test section and indicated that sound was propagating upstream from the diffuser. These observations are described more completely in Section 5.1. The magnitude of the extraneous signal produced by sound in the test section is finally determined in Section 5.1 to be 1/20 of the wall-pressure fluctuations.

3.3. Turbulence in the test section

The wind tunnel does not have a honeycomb but the settling chamber is fitted with four turbulence damping screens. The turbulence level in the center of the test section rises with speed and has been measured at speeds of 50, 100, and 150 ft/sec. By extrapolation to 200 ft/sec, the speed used in the bulk of the present work, the turbulence level of the axial velocity component near the center of the test section is approximately $\frac{\sqrt{\overline{u'^2}}}{U_\infty} = 6 \times 10^{-4}$.

The transverse velocity in the center of the test section is three times the axial velocity, $\sqrt{\frac{\overline{v'^2}}{\overline{u'^2}}} = 3$, at all speeds. If one assumes that the sound field in the test section consists of plane waves propagating in one direction, the root-mean-square velocity fluctuations associated with sound would amount to approximately $\frac{\sqrt{\overline{u'^2}}}{U_\infty} = 10^{-4}$. It seems certain that the majority of the turbulent velocity fluctuations in the test section are produced by vorticity or entropy fluctuations.

Additional information about the turbulence in the wind tunnel near the wall was obtained from the initial wall-pressure measurements beneath the turbulent boundary layer, section 4. After the tunnel was started and the wind-tunnel air had reached an equilibrium velocity, the mean-square wall-pressure fluctuations from 5 to approximately 100 cps were very great but slowly decreased monotonically with time and 30 minutes later reached an equilibrium value that was an order of magnitude lower than the initial value. Examination of the spectrum of these wall-pressure fluctuations showed that the energy density was greatest at low frequencies. It was also noticed that the mean-square and low-frequency spectrum of the wall-pressure fluctuations did not decrease after starting the tunnel if the sun was shining. If the tunnel was run at night or on a cloudy day, the mean-square and low-frequency spectrum of the wall pressure would reach low values. On a few occasions, the mean-square wall pressure was observed to decrease as the sun was obscured by clouds and increase again when the sun reappeared.

The streamlines near the wall in the contraction section were observed using the dense white smoke produced when titanium tetrachloride is exposed

to air. Large-scale oscillations of the streamlines near the wall were observed above the concave surface of the contraction section. The large-scale eddies produced in the contraction section were carried into or just above the test-section boundary layer. We believe that low-frequency, large-scale flow disturbances are produced by the combined effects of Taylor-Goertler boundary-layer instability and density stratification of the air near the wind-tunnel wall. Density stratification is produced by heat transfer through the steel shell of the wind tunnel. When the density-stratified air is accelerated into the test section, vorticity is produced and causes the large-scale, low-frequency wall-pressure fluctuations.

Examination of many wall-pressure spectra showed that above approximately 100 cps the spectra are always repeatable and independent of the temperature of the wind-tunnel shell.

3.4. The nature of the turbulent boundary layer used in the investigation

The turbulent boundary layer developed on the lower surface of the test section was used in the investigation. Figure 1 shows the dimensions of the lower surface of the wind-tunnel contraction and test section. The lower surface of the test section was covered with sheets of varnished masonite to provide a smooth surface for the development of the boundary layer. The majority of the measurements were made at a speed of 200 ft/sec, and all with natural transition of the boundary layer.

To allow the results of this investigation to be repeated or compared with other experiments, the properties of the turbulent boundary layer in the test section must be investigated and compared with an accepted standard for

the equilibrium turbulent boundary layer. The ideal turbulent boundary layer of Cole's (1953) was selected as the standard.

The properties of the turbulent boundary layer were measured with a Stanton tube and a Pitot tube. The shearing stress at the wall was obtained from the Stanton tube measurements using the data and results of Stanton tube calibration presented by Bradshaw and Gregory (1961). From the Pitot tube measurements the mean velocity profile, boundary-layer thickness, displacement thickness, and momentum thickness were obtained.

These measured properties of the boundary layer are tabulated and compared in table I with the properties that the ideal boundary layer would have

TABLE I

PROPERTIES OF THE ACTUAL AND IDEAL TURBULENT BOUNDARY LAYER

Boundary Layer	U_∞ ft/sec	R_θ	δ	δ^*	θ	δ^*/θ	U_τ/U_∞	R
Actual	204	38,000	0.42	0.041	0.0315	1.3	0.0326	$3.1\times10^{7*}$
Ideal		38,000				1.3	0.0318	3.2×10^{7}
Actual	156	29,000	0.374	0.038	0.034	1.25	0.0331	$2.5\times10^{7*}$
Ideal		29,000				1.31	0.0325	2.3×10^{7}

*Assumed origin of boundary layer at station 10 of figure 1.

if the Reynolds number based on momentum thickness, R_θ, were the same. The velocity profiles have been plotted in figure 3, where the velocity profile of the ideal boundary layer is also shown. Examination of table I and figure 3 shows that the properties of the boundary layer at 204 ft/sec agree reasonably

well with the properties of the ideal boundary layer. At 150 ft/sec, the value of the measured shape parameter, displacement thickness divided by momentum thickness, δ^*/θ, is considerably lower than the value of the ideal shape parameter, and some deviation from the ideal velocity profile is also apparent in figure 3. Apparently, the boundary layer with natural transition has not completely reached an equilibrium state at the speed 150 ft/sec. The turbulent boundary layer produced by natural transition at 200 ft/sec was judged to represent a reasonable approximation to the ideal turbulent boundary layer and was used for the majority of the wall-pressure measurements. A few measurements of mean-square wall-pressure fluctuations were made beneath boundary layers that were tripped or developed on a rough surface. The properties of these boundary layers are discussed along with the measurements of the fluctuating wall pressure beneath them in section 4.2.

4. ROOT-MEAN-SQUARE AND POWER SPECTRUM OF THE WALL PRESSURE

The wall pressure is a stationary random function of time, t, and position x, z. We use the theory of stationary random functions to interpret the pressure fluctuations that are measured. The quantities measured are the correlation or covariance of the pressure

$$R_{pp}(x_1,x_3,\tau) = \frac{\overline{p(x,z,t)p(x+x_1,z+x_3,t+\tau)}}{\sqrt{\overline{p^2(x,z,t)}\ \overline{p^2(x+x_1,z+x_3,t+\tau)}}} \qquad (1)$$

and the temporal Fourier transform of the auto correlation of the pressure defined by

$$\overline{p^2}R_{pp}(0,0,\tau) = \int_0^\infty E(\omega)\cos\ \omega\tau d\omega \qquad (2)$$

with the inverse

$$E(\omega) = (\pi)^{-1} \int_0^\infty \overline{P^2}R_{pp}(0,0,\tau)\cos\ \omega\tau d\tau \qquad (3)$$

$E(\omega)$ is the power spectrum of the pressure.

When the first measurements of the wall pressure were made, it was found that the power spectrum of the pressure fluctuations contained a large energy density at low frequencies which varied from day to night and also when the amount of sunlight shining on the tunnel changed during the day. For example, we have obtained spectra measured on the same day with different amounts of sunlight and have found differences between the spectra amounting to a factor of ten or more at frequencies below $\frac{\omega\delta^*}{U_\infty} = 0.05$ (40 cps). The variation in the pressure spectrum at low frequencies is attributed to density stratification of the air near the wind-tunnel wall as already discussed in section 3.3. The spectra of the wall pressure above a dimensionless frequency $\frac{\omega\delta^*}{U_\infty} = 0.14$ were always repeatable and scaled with the wind-tunnel speed and boundary-layer-displacement thickness. Therefore the present experiments were restricted to frequencies produced by the fluctuating pressures in the boundary layer above $\frac{\omega\delta^*}{U_\infty} = 0.14$.

In the measurements of the mean-square pressure and space-time correlation of the pressure, we used the Krohn-Hite filter to reject all frequencies below $\frac{\omega\delta^*}{U_\infty} = 0.14$. For the boundary layer developed at 200 ft/sec, with displacement

thickness $\delta^* = 0.041$ ft, and thickness $\delta = 0.42$ ft, the wave length associated with a convected eddy that produces pressure fluctuations at $\frac{\omega\delta^*}{U_\infty} = 0.14$ is 3.98. Thus we can certainly obtain information about eddies whose scale is of the order of one or two boundary-layer thicknesses even when we reject signals below $\frac{\omega\delta^*}{U_\infty} = 0.14$.

4.1. Boundary layers developed on a smooth surface with natural transition

The power spectra of the wall-pressure fluctuations measured at 150 and 200 ft/sec, with natural transition on a smooth surface, are shown in figure 4. The vertical dashed line shows the dimensionless frequency $\frac{\omega\delta^*}{U_\infty} = 0.14$ below which the spectra were not always repeatable. The dimensionless spectra of figure 4 at 150 ft/sec agree very well with the spectra obtained at 200 ft/sec, even though the boundary-layer shape parameter at 150 ft/sec does not agree with the ideal boundary-layer shape parameter.

The root-mean-square wall pressure was measured on ten different occasions at 200 ft/sec, and on five different occasions at 150 ft/sec, over a frequency band $0.14 < \frac{\omega\delta^*}{U_\infty} < 28$. The average of the wall-pressure measurements was corrected for the effect of extraneous signals from the transducer. From the tests of sound, vibration, and turbulence in the wind tunnel, we estimate that approximately 1/20 of the measured mean-square-wall pressure fluctuations are produced by extraneous signals which are uncorrelated with the turbulent pressure fluctuations in the boundary layer. The extraneous signals are caused primarily by upstream propagating sound in the test section as explained in sections 3.2 and 5.1.

The corrected value of the root-mean-square wall pressure is $\sqrt{\overline{p^2}}/\tau_w = 2.19$

at 200 ft/sec, and $\sqrt{\overline{p^2}}/\tau_w = 2.15$ at 150 ft/sec.

4.2. Increase in the root-mean-square wall pressure and power spectrum caused by surface roughness and a boundary-layer trip

The value of the root-mean-square wall pressure reported in the previous section was exceeded when the boundary layer was tripped or developed on a rough surface.

The surface roughness was produced by machine tool marks on the unlapped surface of the 20-in.-diameter steel disk in which the transducers were mounted and by slight misalignment (±0.004 in.) of the dummy transducers in their holes upstream of the transducer. Elsewhere, the wall was smooth and in the same condition as it was for the measurements of section 4.1. The wall-pressure measurements and the properties of the boundary layer are shown in table II.

TABLE II

EFFECT OF WALL ROUGHNESS ON WALL-PRESSURE FLUCTUATIONS

$\sqrt{\overline{p^2}}/q_\infty \times 10^3$	$\sqrt{\overline{p^2}}/\tau_w$	U_∞	U_∞/U_τ	$\Delta U/U_\tau$	CONDITION
4.66	2.19	204	30.7	0	Smooth Plate
7.0	3.09	205	29.7	-2.36	Rough Plate
4.7	2.15	156	30.1	0	Smooth Plate
6.6	2.63	153	28.2	-2.36	Rough Plate

The quantity $\Delta U/U_\tau$ is the amount that the logarithmic portion of the mean velocity profile of the boundary layer was displaced from the equilibrium velocity

profile of figure 3 when the surface was rough. The change in the boundary-layer turbulence caused by the roughness results in an increase in fluctuating wall pressure and wall shear. However, the increase in wall shear is not as great as the increase in the fluctuating wall pressure (see table II). The power spectrum of the wall-pressure fluctuations on the rough surface was also measured and was increased, at all frequencies, by the ratio of the mean-square pressures measured on rough and smooth surfaces. The pressure-fluctuation measurements on the rough steel disk demonstrate that surface roughness on even a small portion of the wall can have a profound effect on the fluctuating wall pressure in the immediate vicinity.

We can illustrate the effect of surface roughness everywhere on the wall and other disturbances in the boundary layer from the results of tests made at the beginning of this investigation. A two-dimensional boundary-layer trip (a square 1/2- x 1/2-in. strip of wood) was placed on the wall 9 feet ahead of the transducer. In this case the wall was already rough everywhere (rough, unfinished plywood) and the steel plate was rough as described above. The root-mean-square wall pressure before the trip was in place was $\sqrt{\overline{p^2}}/q_\infty = 0.008$ but increased to $\sqrt{\overline{p^2}}/q_\infty = 0.0097$ when the trip was in place. In this case also, the power spectrum with the trip and a rough wall was almost the same as the power spectrum shown in figure 4, if the power spectrum of figure 4 at each frequency is multiplied by the ratio of the appropriate mean-square pressures. Unfortunately, we are unable to relate the root-mean-square wall pressure to the wall shear stress because the mean velocity profile was not correctly measured in these tests with the trip and with roughness everywhere on

the wall.

4.3. Root-mean-square wall-pressure measurements of this and other investigations

Any comparison of measurements of the root-mean-square wall pressure must be interpreted in the light of the effects that Reynolds number, surface roughness, and other disturbances can have on the fluctuating pressure. Table III shows the results of this and a number of other investigations of fluctuating wall pressures. We do not know enough about the experimental environment in most of the other investigations to decide why different values of $\sqrt{\overline{p^2}}/\tau_w$ were observed. The results of Corcos (1962) show quite clearly that in a tube the ration $\sqrt{\overline{p^2}}/\tau_w$ slowly decreases as the Reynolds number increases. Reliable measurements in a boundary layer with systematic variation of the Reynolds number have not yet been reported.

5. LONGITUDINAL SPACE-TIME CORRELATION OF THE WALL PRESSURE

5.1. The measurements of the longitudinal space-time correlation of the wall pressure

The correlation $R_{pp}(x_1,0,\tau)$ of the wall pressure measured at two points, one directly downstream of the other but separated by a distance, x_1, in the stream direction was investigated at a free-stream speed of 200 ft/sec. The pressure signals from the two transducers were recorded simultaneously on magnetic tape and were played back with a variable time delay of one signal with respect to the other. The correlation $R_{pp}(x_1,0,\tau)$ between the time-delayed pressure signals for various spatial separations, x_1, and time delays,

TABLE III

SUMMARY OF SOME RESULTS OF WALL-PRESSURE MEASUREMENTS BENEATH TURBULENT BOUNDARY LAYERS

$\sqrt{\overline{p^2}}/\tau_w$	$\sqrt{\overline{p^2}}/q_\infty \times 10^3$	Re_θ	Source	Remarks
3.24	9.5	3,800	Harrison(1958)	Extraneous noise not known
2.32	5.5	13,000	Willmarth(1959)	Transducer too large. $d/\delta^*=1.1$
2.49	5.7	22,600		Boundary layer tripped
0.97	1.9	65,000	Skudrzyk and Haddle(1960)	Measured in water. Large transducer, $d/\delta^*=2.5$
3.5	Unknown	Unknown	Kistler	Reported by Laufer (1961)
2.15	4.7	29,000	Present	Relatively small transducer,
2.19	4.66	38,000	Investigation	$d/\delta^*=0.33$
2.5	Not Applicable		Corcos(1962)	$Re_d=6\times10^4$ Turbulent flow
2.0				$Re_d=2\times10^5$ in a tube

τ, are shown in figure 5. In this figure the origin $\tau = 0$ (indicated by a short vertical line) has been shifted to the left to display the maxima of the wall-pressure correlations beneath each other. The pressure-fluctuation signals were filtered so that only frequencies from $105 < f < 10{,}000$ cps ($0.14 < \frac{\omega\delta^*}{U_\infty} < 13.6$) are included in the measurements.

Some remarks about the effect of the filter on the pressure correlation are necessary. First, the value of $R_{pp}(x_1,0,\tau)$ is not changed appreciably by

the high-frequency cutoff at 10,000 cps where the power spectral density is small (see figure 4). The low-frequency cutoff at 105 cps produces the major effect. The magnitude of this effect can only be estimated because the true power spectrum of the pressure is masked by the low-frequency pressure fluctuations produced by large-scale density stratification in the boundary layer.

If we assume that the power spectrum of the pressure below 105 cps is constant and equal to the value at 105 cps, the measured value of the autocorrelation of the pressure $R_{pp}(0,0,\tau)$ of figure 5 can be corrected using equation (2). The corrected value of $R_{pp}(0,0,\tau)$ has been computed and is shown in figure 11 where it is presented as a spatial correlation in a moving reference frame with $\tau = x_1/U_c$. The corrected value of $R_{pp}(0,0,\tau)$ is unchanged at $\tau = 0$, does not oscillate, and is greater than the measured autocorrelation for all τ. The greatest correction to the measured autocorrelation occurs over the range $2 < \frac{\tau U_\infty}{\delta^*} < 16$ and causes an increase of 14% at most.

If it is assumed that the power spectrum of the pressure below 105 cps falls linearly to zero at $\omega = 0$, the corrected autocorrelation is at most 6% greater than the measured autocorrelation of figure 5. The corrected autocorrelation will now oscillate because $E(\omega) = 0$ [see equation (3)]. The first and only zero crossing of the autocorrelation of the pressure occurs at $\tau U_\infty/\delta^* = 5$ instead of 3.

We must conclude that the nature of the spectral density of the pressure below 105 cps will control the behavior of the tail of the pressure correlation; however, the maxima of the pressure correlation are not appreciably affected by the filter. The correlation measurements of figure 5 show that

the wall-pressure fluctuations appear to be convected downstream, $\tau > 0$, at a fraction greater than 1/2 of the stream speed. A small portion of the wall-pressure fluctuations appear to be moving upstream, $\tau < 0$, at a much higher speed, approximately 1200 ft/sec. The upstream propagation of pressure fluctuations is undoubtedly caused by sound waves produced in the wind-tunnel diffuser and fan, which travel upstream through the test section towards the settling chamber. We have determined the frequency of the upstream propagating sound field by filtering out pressure signals at low frequencies, and measuring the correlation $R_{pp}(x_1,0,\tau)$ over the restricted frequency range $300 < f < 10{,}000$ cps $\left(0.41 < \frac{\omega\delta^*}{U_\infty} < 13.6\right)$. In this case there was no longer any correlation between the wall pressures when τ is less than zero and x_1 is large. Therefore the majority of the sound pressure is produced by sound waves with a frequency below 300 cps. The measurements of the power spectrum of the wall pressure, figure 4, at 206 ft/sec, show small peaks apparently caused by the upstream propagating sound in the frequency band $105 < f < 300$ cps $\left(0.14 < \frac{\omega\delta^*}{U_\infty} < 0.41\right)$. The mean-square sound pressure in the test section can be estimated from the average maximum value of $R_{pp}(x_1,0,\tau)$ for $\tau < 0$ (approximately $R_{pp}(x_1,0,\tau) = 0.05$). This value of $R_{pp}(x_1,0,\tau)$ is approximately the ratio of mean-square sound pressure in the test section to mean-square pressure measured by the transducer. We have used this value in section 4.1 to estimate the true value of the root-mean-square wall pressure.

To display the correlation measurements in space, $\frac{x_1}{\delta^*}$, and time delay, $\frac{\tau U_\infty}{\delta^*}$, a three-dimensional drawing, figure 6, of the wall-pressure correlation has been constructed from the data of figure 5.

5.2. Convection speed of large- and small-scale pressure producing eddies

The measured correlations displayed in figure 6 suggest that in a frame of reference, moving in the stream direction, $x_1 > 0$, $\tau > 0$, the time variation of the wall pressure would be reduced. One can define an integral time scale and by quadratures determine the (constant) velocity of a frame of reference in which the time scale is the greatest [Phillips (1957)]. We shall not define an integral time scale but will consider instead the trajectory in space and time of a reference frame in which the decay of the pressure correlation at each time delay is the least. This trajectory will correspond to the average trajectory of an observer who follows the pressure-producing eddy systems as they move downstream and decay. The trajectory, in the x_1, τ plane, of the reference frame in which the decay of R_{pp} is the least is the locus of points on the lines R_{pp} = const. which have the greatest value of τ. This trajectory is shown as a heavy solid line on the contour map of the pressure correlation, figure 7, which was obtained from the data of figure 5. The slope, $dx_1/d\tau$, of the trajectory shown in figure 7 may be considered to be the speed of the reference frame in which the rate of decay of a given pattern of wall pressure is the least. When x_1 or τ are small the speed of the reference frame is less than it is for larger spacings, x_1, or later times, τ. The increase in speed of the reference frame is caused by the decay of small pressure-producing eddies near the wall where the mean speed is low. When the smaller eddies have decayed, the observer interested in a certain initial pressure configuration must move faster to keep up with the more rapidly moving large-scale remnants of the original pressure pattern. Eventually (x_1,τ large) nothing

of the original configuration remains and $R_{pp} = 0$. The speed of the reference frame in which the rate of decay of the pressure correlation is the least will be called the convection speed of the pressure-producing eddies and will be considered to be a function of x_1/δ^*. Figure 8 shows the convection speed obtained from the slope of the heavy line in figure 7. The convection speed varies from $\frac{U_c}{U_\infty} = 0.56$ when $x_1/\delta^* = 0$ to an asymptotic value $U_c/U_\infty = 0.83$ for large x_1/δ^*. The asymptotic value of the convection speed might be somewhat greater if low-frequency pressure fluctuations produced by large eddies had not been rejected by the filter. (Wave lengths greater than 3.9δ have been rejected.)

The pressure correlation in a frequency band centered at low and at high frequencies has been investigated. The correlation in a frequency band was measured by passing the sum and then the difference of the two pressure signals through the band pass filter before the sum and difference signals were squared and averaged by the thermocouple. The passage of any pair of correlated random signals through a band pass filter will produce oscillations of the correlation between the signals. A classical example is the diffraction of light by a slit. It may be unnecessary to remark that in general the structure of the correlation between two signals passed through a narrow band filter is more dependent on the characteristics of the filter than on the characteristics of the original signal. We must not attach any deep significance to oscillations of the pressure correlation produced by the filter.

The pressure correlation in two frequency bands, $300 < f < 700$ cps and $3000 < f < 5000$ cps, was measured as a function of x_1 and τ. Most of the sound

in the test section is below 300 cps and cannot affect these measurements. The pressure correlation in each frequency band was normalized by dividing by the autocorrelation of the pressure, $R_{pp}(0,0,\tau)$, in that frequency band. For any particular spacing, $x_1 > 0$, between the transducers, the correlation function in a given frequency band is an oscillating function of τ. As τ is increased, the correlation function oscillates with increasing amplitude until a maximum amplitude is reached and then oscillates with decreasing amplitude until it vanishes. Figure 9 shows only the peak of maximum amplitude of the correlation function for each transducer spacing x_1. Numerous experimentally measured points have not been shown on this plot. In general the scatter was quite small, $\leq 5\%$.

An approximate convection speed of large and small eddies may be obtained from the values of x_1 and τ where the correlation peaks are tangent to their envelope. Figure 8 shows the speed of a reference frame (convection speed) moving with the eddies that produce low- and high-frequency pressure fluctuations. The convection speed in either frequency band is lower when x_1 is small and rises as x_1 increases, presumably because the chosen frequency bands were not narrow enough to isolate completely a single eddy size. However, all the convection speeds in the high-frequency band are lower than those in the low-frequency band. The asymptotic value of the convection speed is $U_c/U_\infty = 0.69$ in the frequency band of from 3000 to 5000 cps ($4.1 < \frac{\omega\delta^*}{U_\infty} < 6.8$) and $U_c/U_\infty = 0.83$ in the frequency band of from 300 to 700 cps ($0.41 < \frac{\omega\delta^*}{U_\infty} < 0.95$). These different convection speeds show that large pressure-producing eddies move faster on the average than smaller eddies (assuming that low- and high-frequency pressure

fluctuations are caused by large and small eddies, respectively).

5.3. Decay of large- and small-scale pressure-producing eddies

The envelopes of the peaks of maximum pressure correlation in low- and high-frequency band (see figure 9) show that the pressure correlation in a high-frequency band decays more rapidly (with increasing x_1) than the correlation in a low-frequency band. We can put this observation on a more definite basis by considering the pressure correlation and spectra in a moving reference frame.

Consider the temporal Fourier transform $F(x_1,0,\omega)$ of the pressure correlation $R_{pp}(x_1,0,\tau)$ defined as

$$R_{pp}(x_1,0,\tau) = \int_{-\infty}^{\infty} F(x_1,0,\omega)e^{i\omega\tau}d\omega \qquad (4)$$

Let us define a coordinate system x',y',z' whose origin moves downstream at the convection speed of the eddies which produce the pressure fluctuations. We also define x' positive in the upstream direction. The spatial separation of the pressure transducers in the fixed and moving systems is related to the time delay between signals from the transducers by

$$\tau = \frac{x_1+x_1'}{U_c} \qquad (5)$$

where x_1 and x_1' are the spatial separations in the fixed and moving systems, respectively. If we assume that the pressure fluctuations are produced by a convected pattern of eddies which changes slowly with time, the frequency of signals observed in the stationary frame is related to the wave number of the convected pressure pattern by $\omega = U_c k$. Under this transformation, equation (4)

becomes the spatial correlation of the pressure in a moving reference frame.

$$R_{pp}\left(x_1,0,\frac{x_1+x_1'}{U_c}\right) = \int_{-\infty}^{\infty} U_c F(x_1,0,U_c k)e^{ikx_1}e^{ikx_1'}dk \qquad (6)$$

The spatial spectrum function in the moving frame [the inverse of equation (6)]

$$U_c F(x_1,0,U_c k)e^{ikx_1} = \int_{-\infty}^{\infty} R_{pp}\left(x_1,0,\frac{x_1+x_1'}{U_c}\right)e^{-ikx_1'}dx_1' \qquad (7)$$

should not depend on x_1 if the pressure pattern does not change as it is connected downstream. Actually, the spectral function in the moving frame will decay as x_1 increases.

It is possible to measure experimentally the decay of the spectral function in the moving reference frame by evaluating the pressure correlation in the stationary reference frame in a narrow frequency band.

Consider the pressure correlation in the moving reference frame, equation (6), evaluated in a narrow wave number band, $k_1 < k < k_2$, at the origin $x_1' = 0$ of the moving reference frame.

$$R_{pp}\left(x_1,0,\frac{x_1+0}{U_c}\right) = 2\int_{k_1}^{k_2} \mathrm{Re}\left\{U_c F(x_1,0,U_c k)e^{ikx_1}\right\} dk \qquad (8)$$

If the wave number band is small enough, the spectral function in the moving reference frame, equation (7), is approximately constant with respect to k. To examine the decay of the spectral function, we form the ratio of the spectral function at x_1 to the spectral function at $x_1 = 0$, in a narrow wave number band. The ratio is

$$R'_{pp}\left(x_1,0,\frac{x_1}{U_c}\right) = \frac{\mathrm{Re}\left\{F(x_1,0,U_c\bar{k})e^{i\bar{k}x_1}\right\}\Delta k}{\mathrm{Re}\left\{F(0,0,U_c\bar{k})\right\}\Delta k}; \qquad \bar{k} = \frac{k_2+k_1}{2},\ \Delta k = k_2-k_1 \tag{9}$$

This ratio can be obtained experimentally from the maximum value of the pressure correlation in a narrow frequency band divided by the autocorrelation in the frequency band. The peak or maximum values of the normalized pressure correlation measured in a narrow frequency band are displayed in figure 9. It is necessary only to reinterpret ω, $\Delta\omega$, and x_1. If we set

$$\bar{k} = \frac{\bar{\omega}}{U_c} = \frac{\omega_2+\omega_1}{2U_c},\ \Delta k = \frac{\Delta\omega}{U_c} = \frac{\omega_2-\omega_1}{U_c} \tag{10}$$

for each peak value of the normalized pressure correlation of figure 9, we obtain the expression R'_{pp} of equation (9). The peak values of the normalized pressure correlation of figure 9 have been plotted in figure 10.

Figure 10 therefore shows the decay of the spectral function R'_{pp} in the moving reference frame for two wave number bands. We have chosen the asymptotic convection velocity of $U_c/U_\infty = 0.83$ for the low wave number band and $U_c/U_\infty = 0.69$ for the high wave number band. The data plotted in figure 10 show that a given wave number component, which is proportional to $(\text{wave length})^{-1}$, of the pressure pattern is destroyed after traveling a distance of approximately four to six wave lengths. Harrison (1958) was the first to report measurements of the spectral function in a narrow wave number band. He considered frequencies below 2000 cps and found that the special function had decayed after traveling two wave lengths downstream. We are not able to explain the difference between our results and those of Harrison.

Corcos (1962) has also measured the decay of the spectral function in a fully developed turbulent pipe flow. His results are shown in figure 10. The spectral function, R'_{pp}, decays more rapidly in turbulent pipe flow than it does in the turbulent boundary layer and is probably a consequence of the greater influence of the solid boundary on the turbulence developed in a pipe.

6. COMPARISON OF THE TRANSVERSE AND LONGITUDINAL SCALE OF THE PRESSURE FLUCTUATIONS

Measurements of the transverse correlation of the pressure for various spatial separations of the transducers were also made in the frequency band of from 105 to 10,000 cps. The transverse correlation for a large or small transducer separation was found to be a maximum when the time delay was zero. All the transverse correlation measurements have been made with zero time delay.

The results of measurements with zero time delay of both the longitudinal pressure correlation $R_{pp}(x_1,0,0)$ and the transverse correlation $R_{pp}(0,x_3,0)$ are shown in figure 11. The approximate spatial correlation of the pressure in the stream direction that would be measured by an observer moving downstream at the convection speed $0.56\ U_\infty$ is also shown in this figure. The correlation in a moving reference frame was obtained from the measured autocorrelation of the pressure, $R_{pp}(0,0,\tau)$ of figure 5 with $\tau = x_1/U_c$. The measured autocorrelation of figure 5 was approximately corrected for the loss of the low-frequency energy below 105 cps that was rejected by the filter. The correction was made by assuming the power spectrum of the pressure below 105

cps was constant and equal to the value at 105 cps.

The transverse and longitudinal pressure correlation data show that the spatial extent of the pressure correlation over the entire frequency band is approximately the same in directions parallel and transverse to the stream. Favre, Gaviglio, and Dumas (1957) found the scale of the spatial correlation of the streamwise velocity fluctuations, U, to be much larger in the stream direction than in a direction transverse to the stream. Their result does not necessarily conflict with the present measurements of the scale of the wall-pressure fluctuations because Kraichnan (1956b) has shown that the dominant term in the interaction between the turbulence and mean shear which produces the wall pressure is $\rho\frac{\partial U}{\partial y}\frac{\partial v}{\partial x}$. The spatial scale of the correlation of a velocity derivative in the direction of differentiation may be much less than the scale of the velocity correlation itself in the same direction.

The presence of large wave length, $\lambda \approx 6$ ft, sound waves propagating upstream in the free stream may cause the spatial extent of the pressure correlation transverse and parallel to the stream to be overestimated at small values of the pressure correlation. The measurements of figure 11 therefore overestimate the spatial extent of the wall-pressure correlation for large values of x_1 or x_3 where $R_{pp} < 0.1$, but are believed to be accurate for values of $R_{pp} > 0.1$.

Measurements of the spatial correlation transverse to the stream produced by pressure fluctuations in a frequency band centered at low and high frequencies are shown in figure 12. The low-frequency band was chosen slightly above the frequency of the sound in the test section. The pressure correlations

have been normalized by the value of the autocorrelation in the same frequency band. It is apparent that the transverse scale of low-frequency pressure fluctuations is much larger than the transverse scale of the high-frequency pressure fluctuations.

A very crude comparison of the longitudinal and transverse scale of the eddies may easily be obtained. If the decay of the pressure at the convection speed is ignored, the transverse correlation measurements of figure 12 are produced by pressure-producing eddies that have a half wave length in the stream direction of magnitude

$$\frac{\lambda}{2\delta^*} = \pi \frac{U_c}{U_\infty} \left(\frac{\bar{\omega}\delta^*}{U_\infty} \right)^{-1} \tag{11}$$

For the low- and high-frequency band, the half wave length turns out to be $\lambda/2\delta^* = 3.8$ and 0.4, respectively. We may conclude from this and from figure 12 that the transverse and longitudinal scale of both the large and small pressure-producing eddies are of the same order of magnitude.

The authors wish to express their appreciation of many fruitful discussions with Professors A. M. Kuethe, E. G. Gilbert, M. S. Uberoi, and C. S. Yih, and Mr. J. L. Amick. The assistance of R. Enlow and H. Kristen who helped us obtain and evaluate the data is gratefully acknowledged.

ADDENDUM

After this report had been written the authors received a paper reporting the recent measurements of longitudinal space-time correlation and spectra of the wall pressure in a water tunnel by Bull, M. K., and Willis, J. L., 1961, Univ. of Southampton A.A.S.U. Report No. 199. Their measurements arrived too late to be compared in detail with ours, but it can be stated that their work is in agreement with ours on the essential points. They also find an increasing convection velocity with increasing transducer spacing ($0.7 < U_c/U_\infty < 0.85$) and they find $\sqrt{\overline{p^2}}/\tau_w \approx 2.7$.

REFERENCES

Batchelor, G. K. 1950 Proc. Camb. Phil. Soc. 47, 359.

Bradshaw, P., and Gregory, N. 1961 British R. and M. 3202.

Bull, M. K. 1960 Dept. of Aeronautics and Astronautics Report 149, University of Southampton.

Coles, D. 1953 Jet Propulsion Lab. Report 20-69 or 1954 Z.A.M.P. V, 181.

Corcos, G. M. 1959 Meeting of Am. Phys. Soc. Div. of Fluid Dynamics, A.P.S. Abstracts.

Corcos, G. M. 1962 Univ. of Calif. Inst. of Eng. Res. Report, Series 183, No. 1.

Favre, A. J., Gaviglio, J. J., and Dumas, R. 1957 J. Fluid Mech. 2, 313.

Harrison, M. 1958 Hydro. Lab. Rept. 1260, David Taylor Model Basin.

Kraichnan, R. H. 1956a J. Acoust. Soc. Am. 28, 64.

Kraichnan, R. H. 1956b J. Acoust. Soc. Am. 28, 378.

Laufer, J. 1961 Jet Propulsion Lab. Tech. Rept. 32-119.

Lilley, G. M., and Hodgson, T. H. 1960 AGARD Rept. 276.

Phillips, O. M. 1957 J. Fluid Mech. 2, 417.

Uberoi, M. S 1953 J. Aero. Sci. 20, 197.

Skudrzyk, E. J., and Haddle, G. P. 1960 J. Acous. Soc. Am. 32, 19.

Willmarth, W. W. 1958a J. Aero. Sci. 25, 335.

Willmarth, W. W. 1958b Rev. Sci. Inst. 29, 218.

Willmarth, W. W. 1959 NASA Memo 3-17-59W.

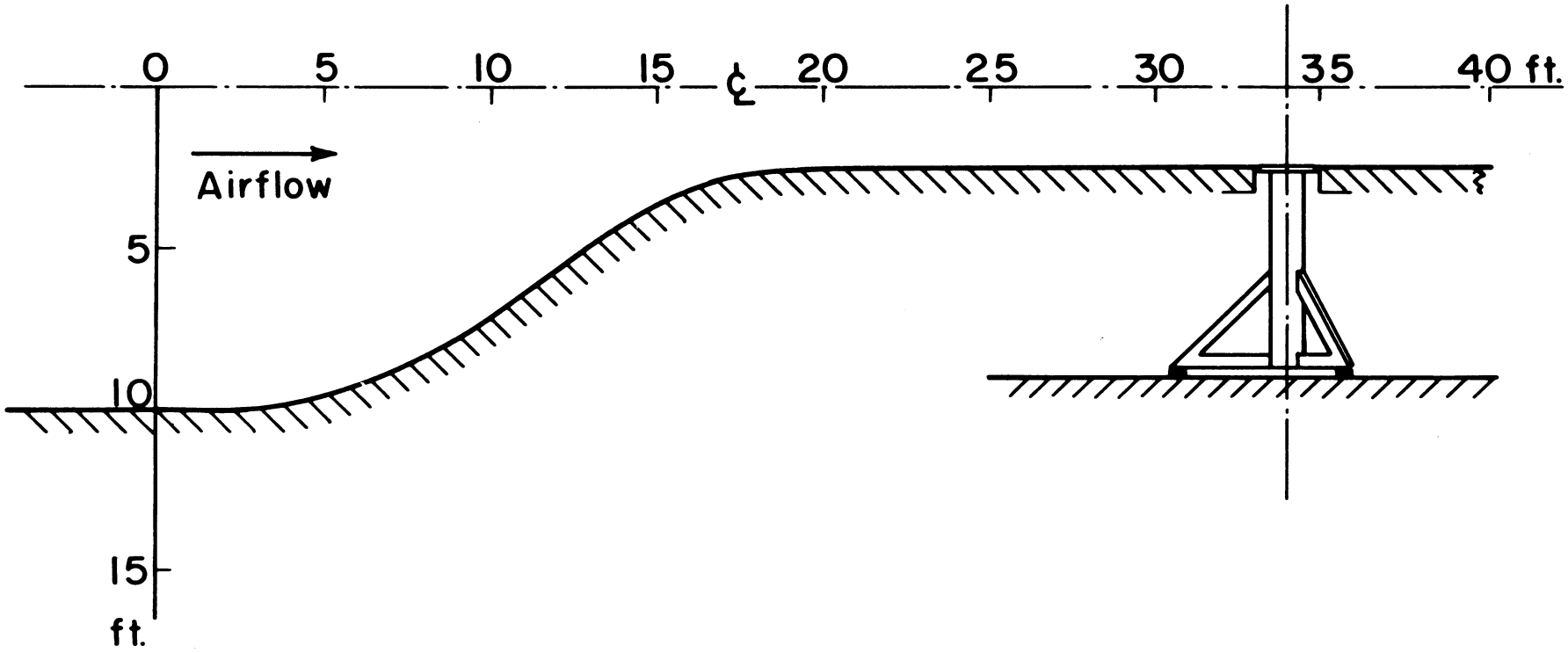

Fig. 1. Scale drawing of wind-tunnel test section and massive vibration isolation mounting for the pressure transducers.

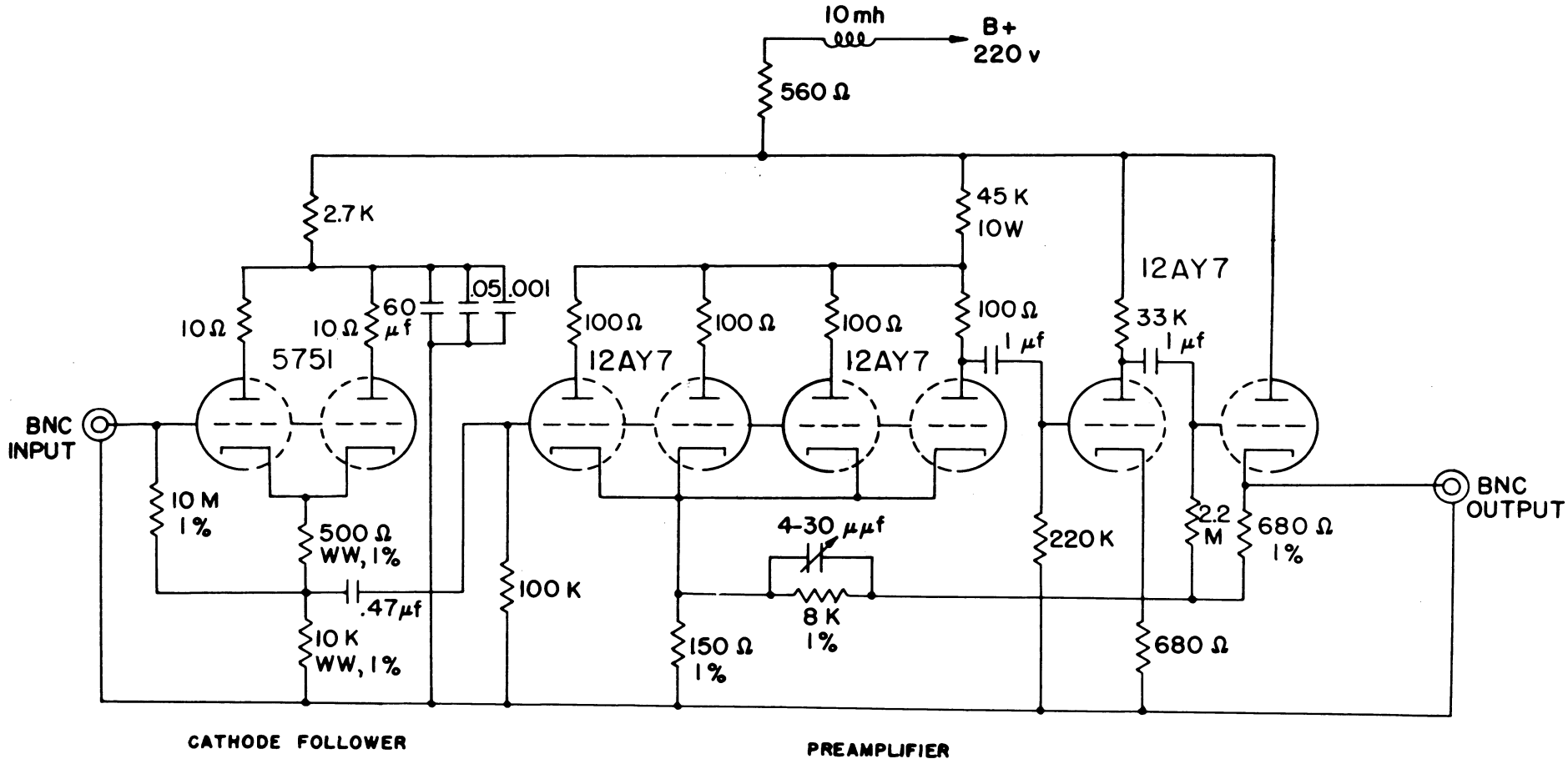

Fig. 2. Circuit diagram for high-input-impedance low-noise cathode follower and preamplifier; input impedance 1.2 x 10^6 ohms; approximate gain is 50.

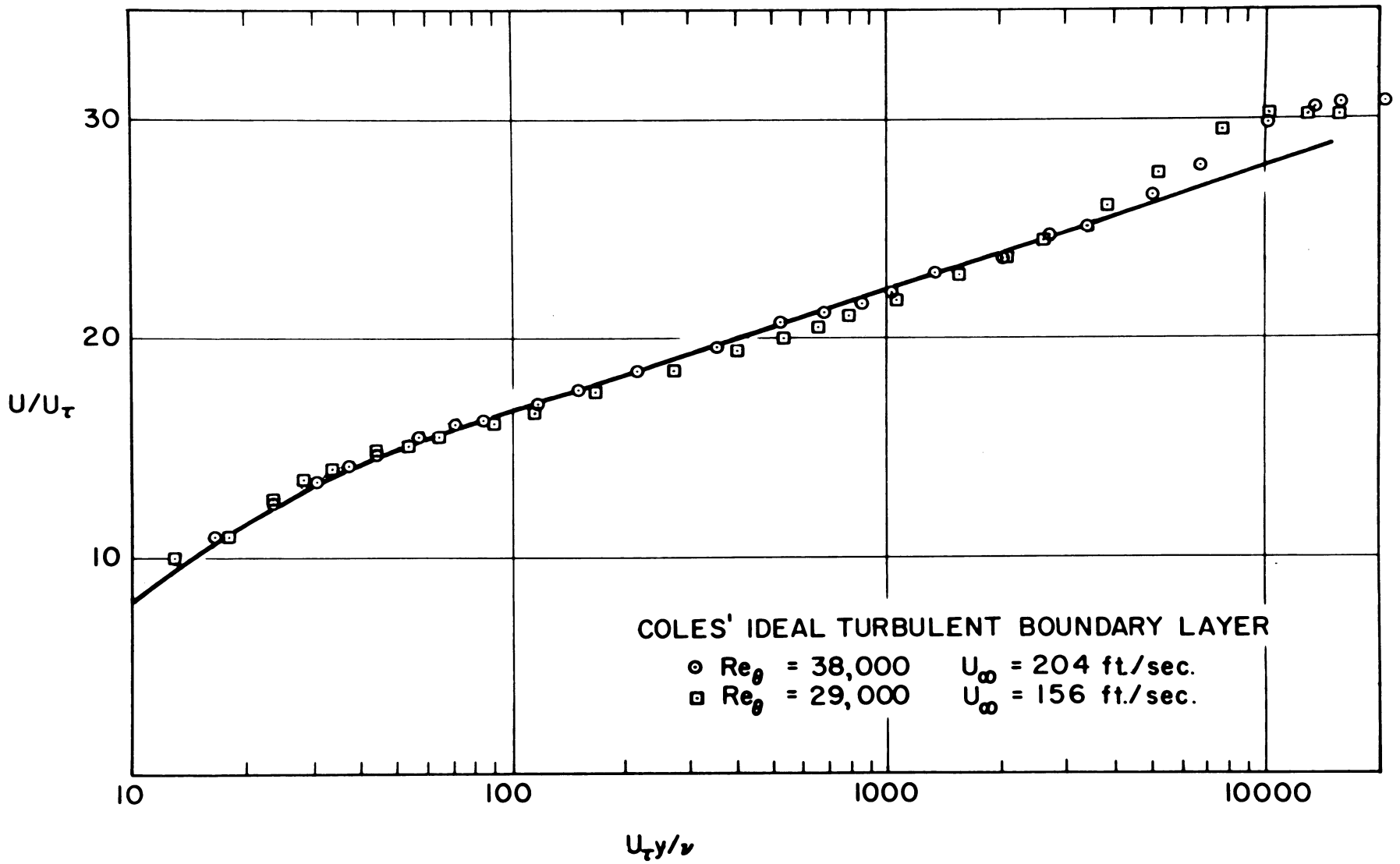

Fig. 3. Mean velocity profiles in the turbulent boundary layer with natural transition. Refer to table I for other parameters describing the boundary layer.

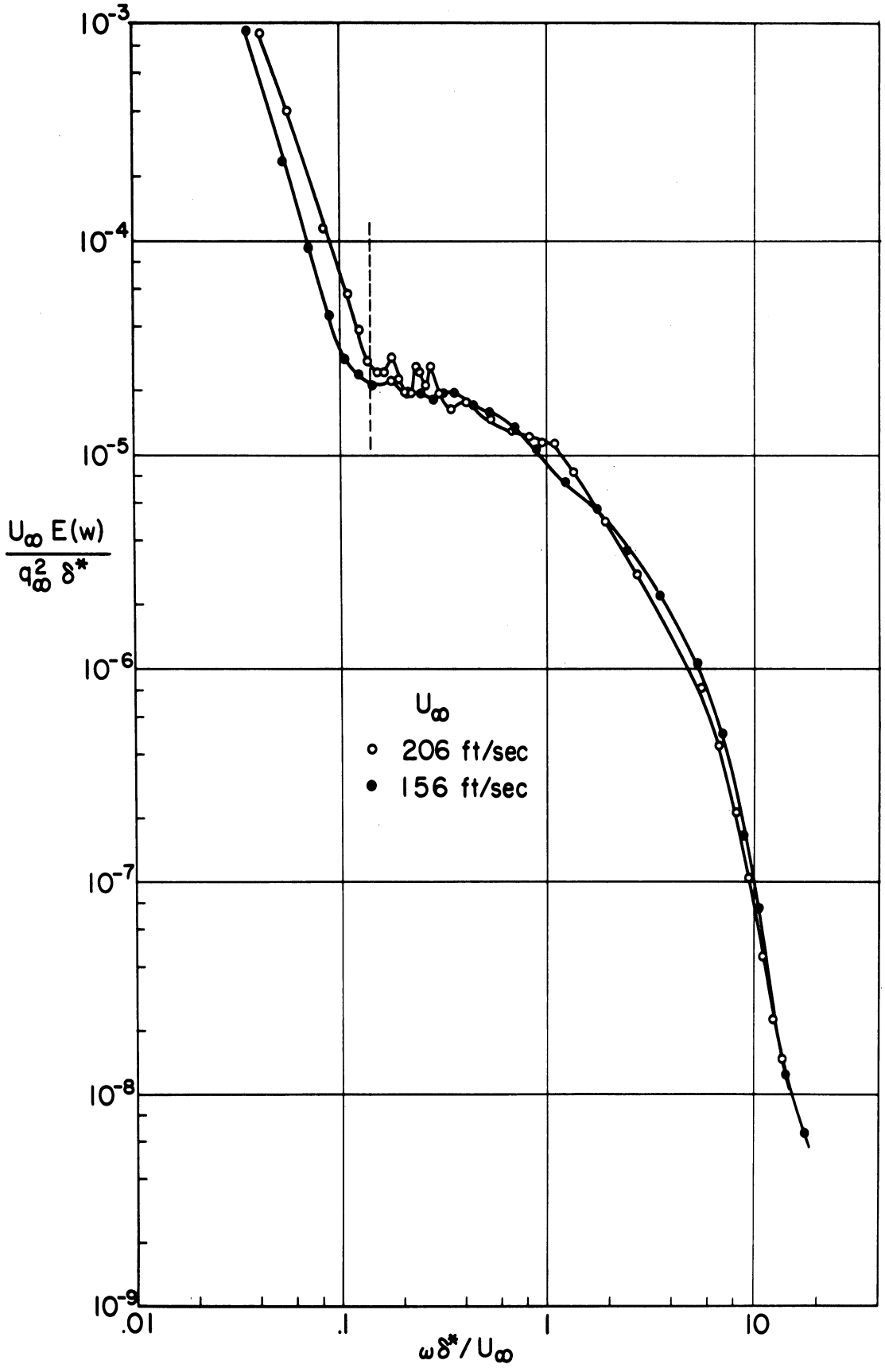

Fig. 4. Dimensionless power spectrum of the wall pressure. Vertical dashed line shows the frequency below which signals were rejected in the subsequent measurements.

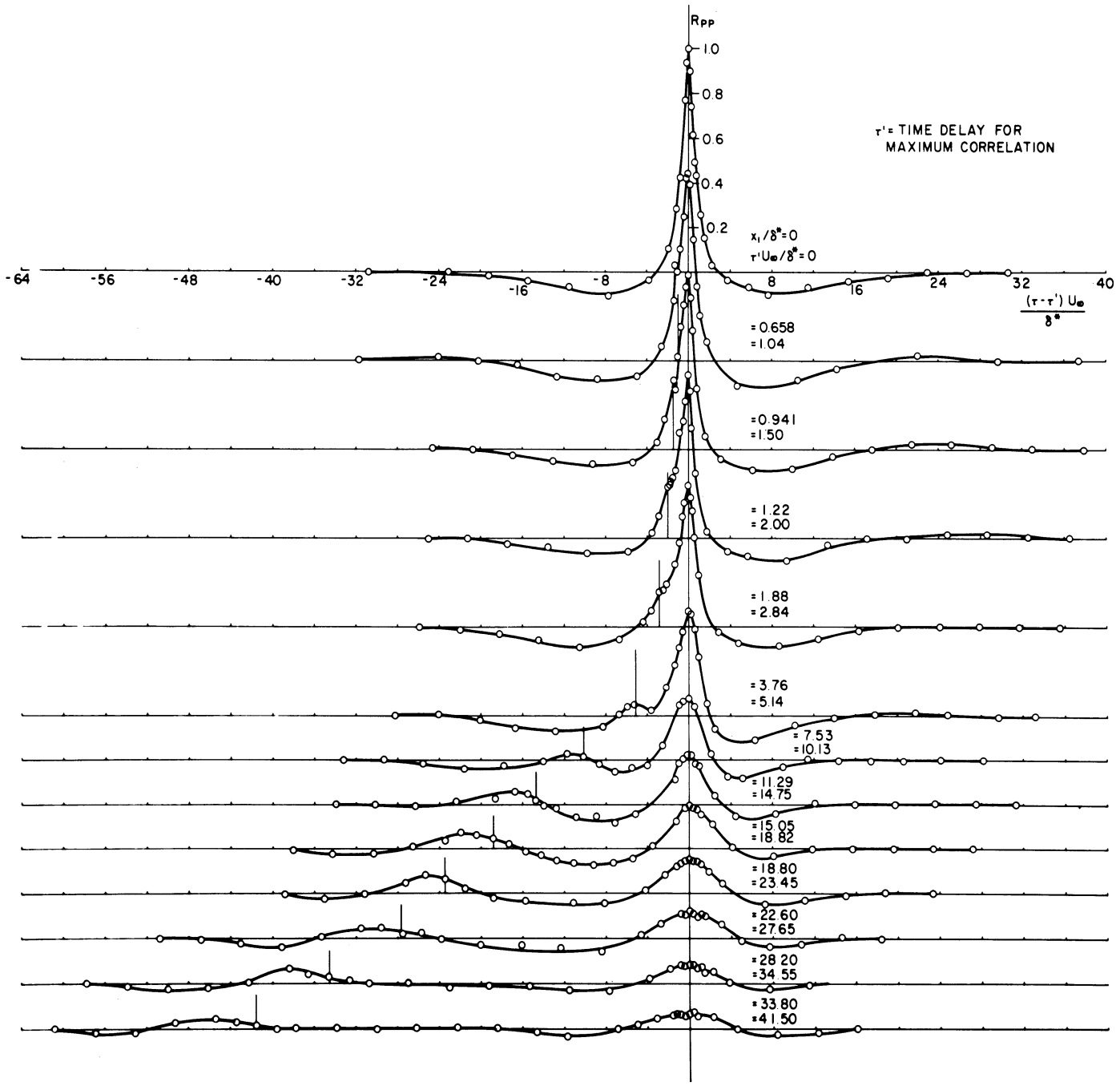

Fig. 5. Measured values of the longitudinal space-time correlation of the wall pressure. The displaced origins, $\tau = 0$, are indicated by a short vertical line.

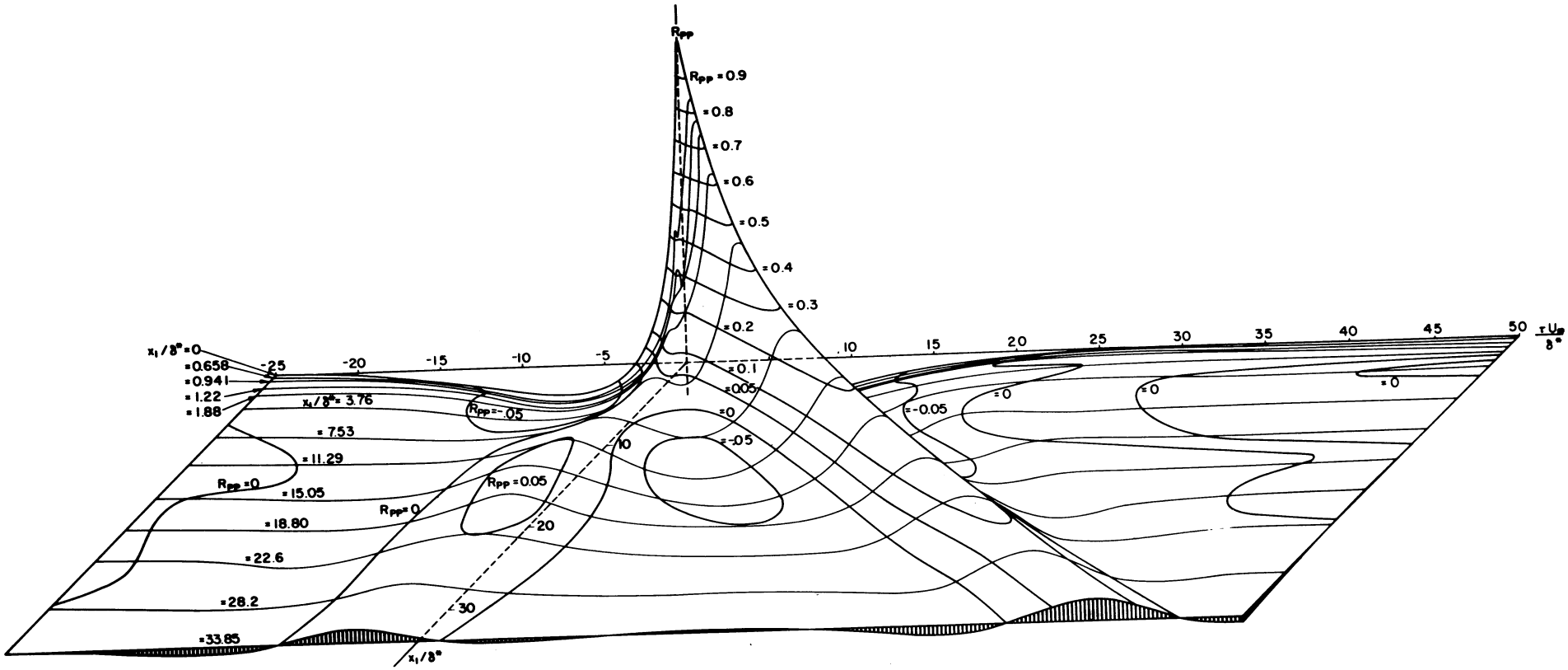

Fig. 6. Longitudinal space-time correlation of the wall pressure displayed in three dimensions using the data of figure 5.

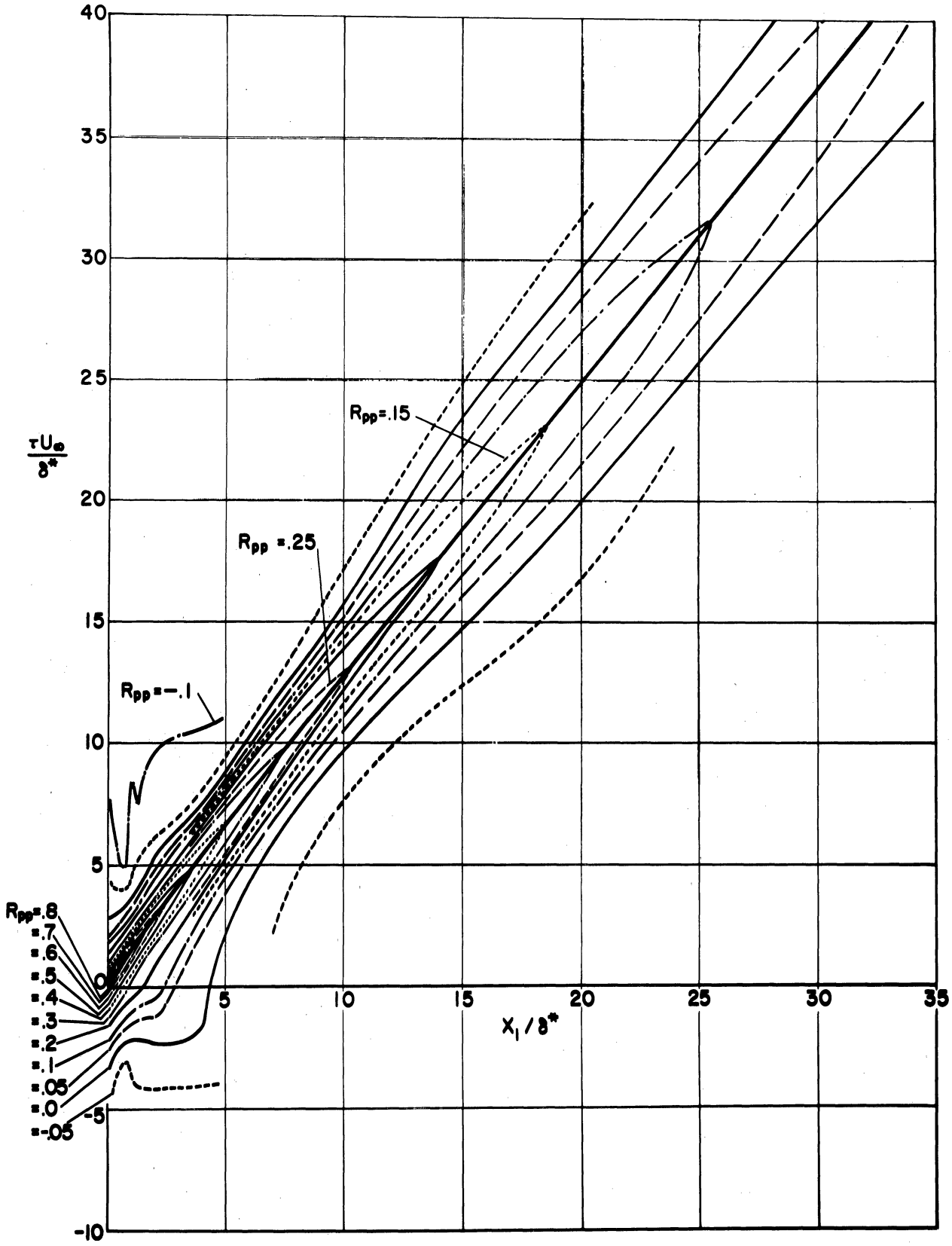

Fig. 7. Contour map of the longitudinal space-time correlation data of figure 5. The heavy line represents the trajectory of a reference frame in which the rate of decay of the pressure correlation is the least.

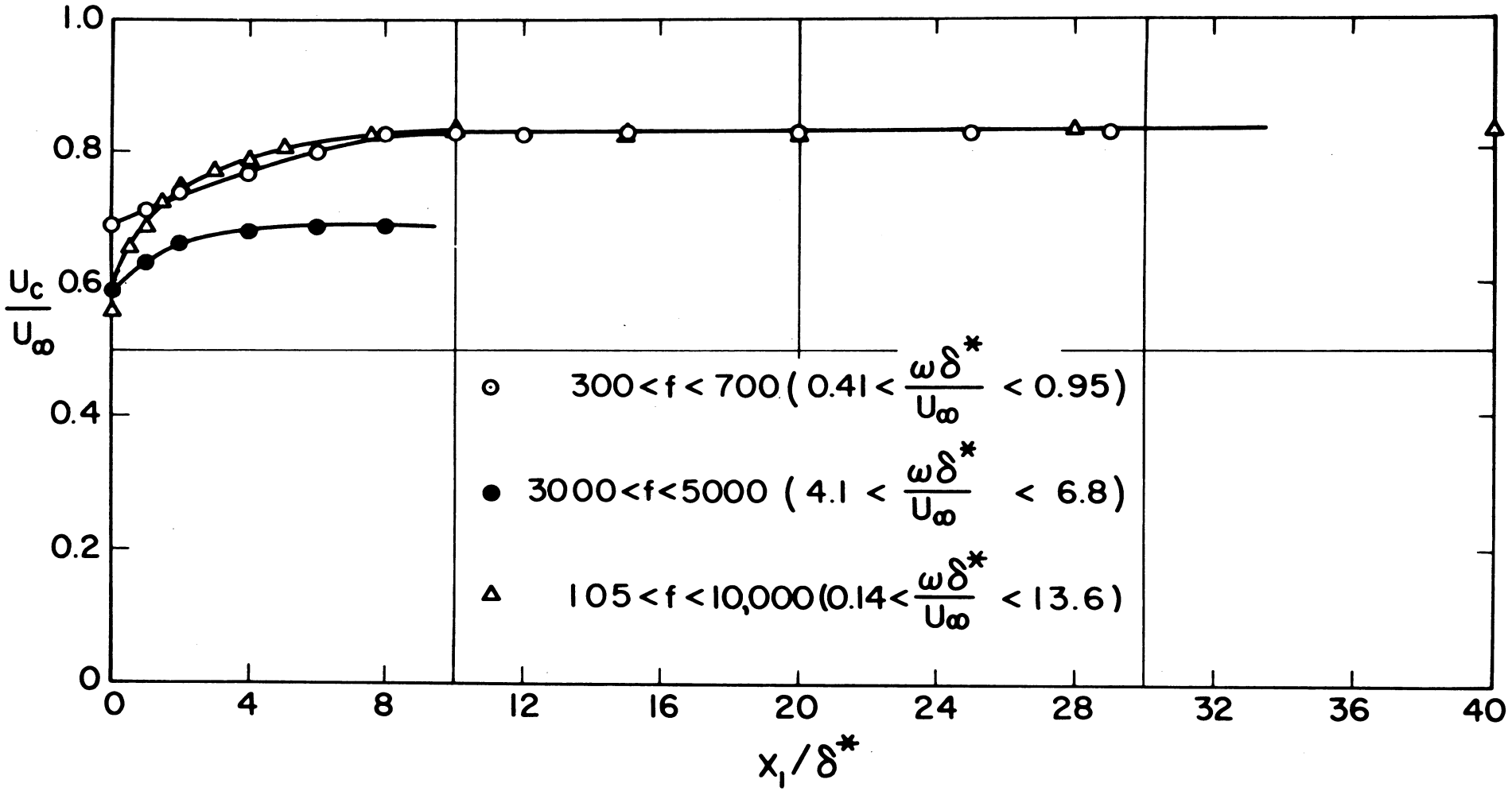

Fig. 8. Local convection speed of pressure-producing eddies for various frequency bands.

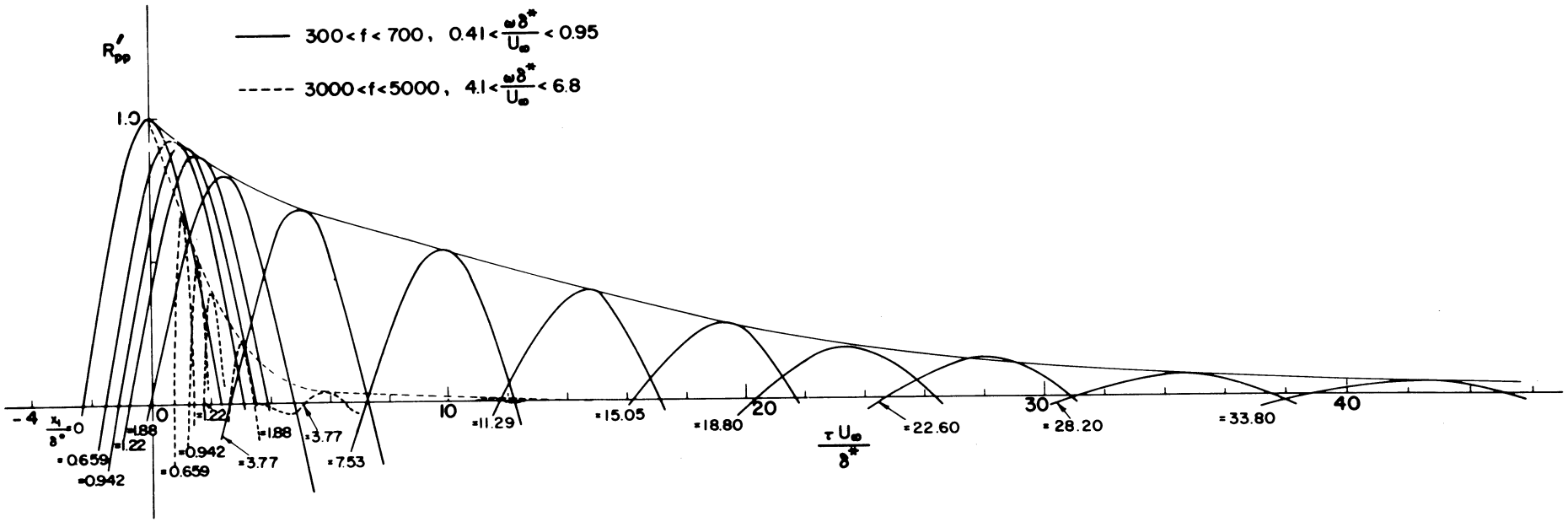

Fig. 9. Peaks of the longitudinal space-time correlation in a low- and a high-frequency band. See equation (9).

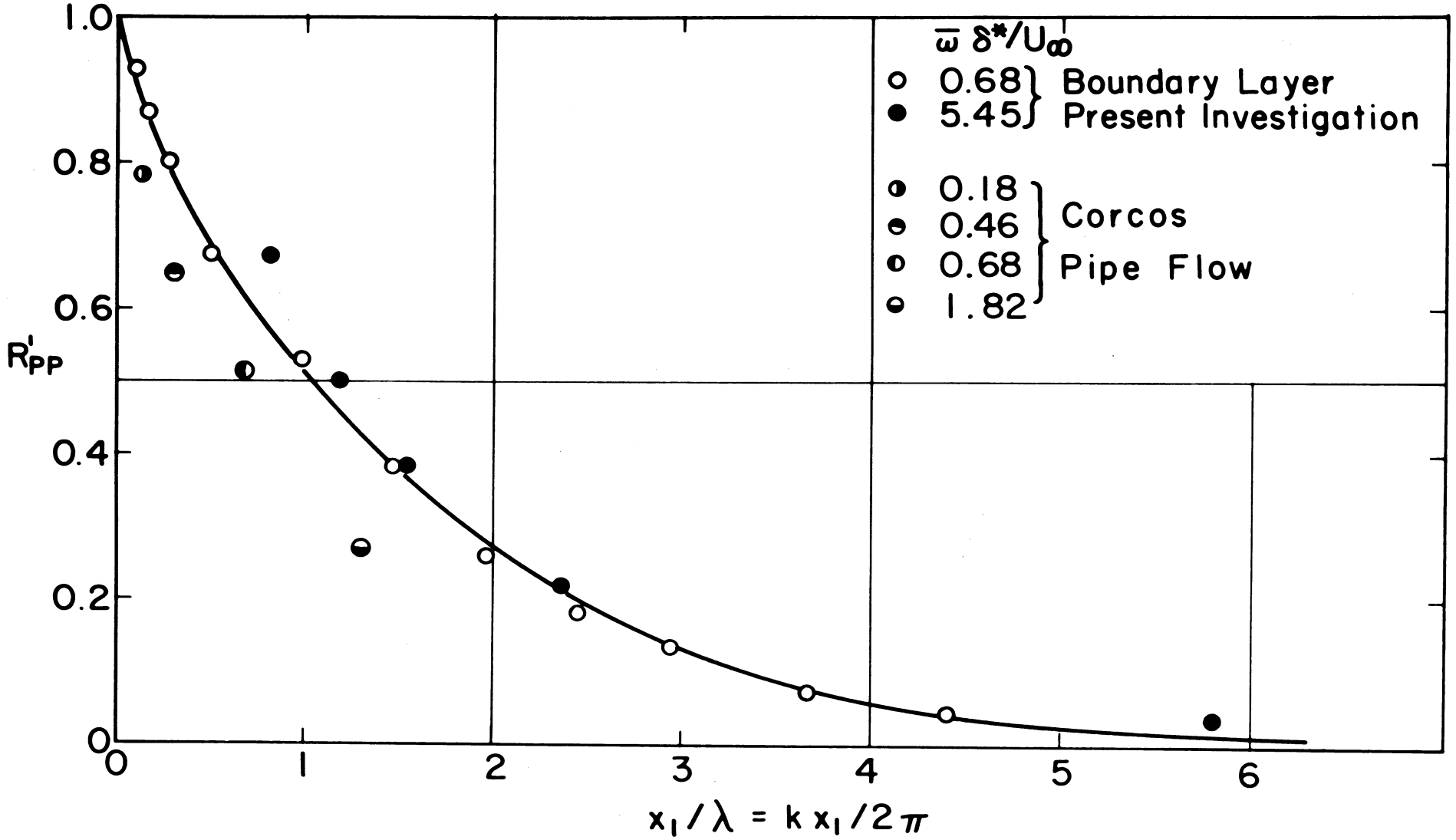

Fig. 10. Decay of large and small wave number components of the wall pressure as measured by an observer moving at the eddy convection speed.

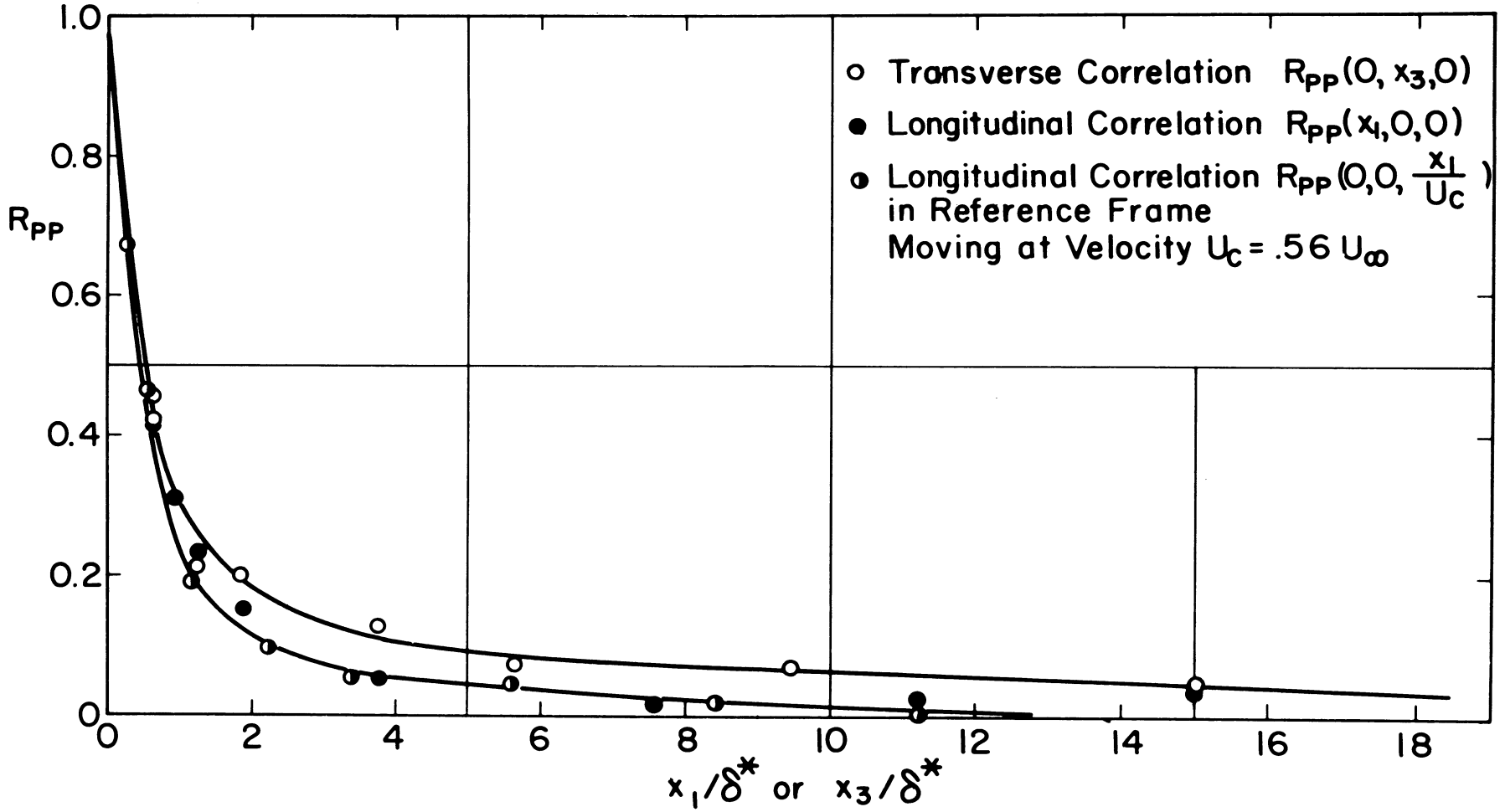

Fig. 11. Transverse and longitudinal spatial correlation of the pressure produced by pressure fluctuations in the frequency band $105 < f < 10{,}000$ cps.

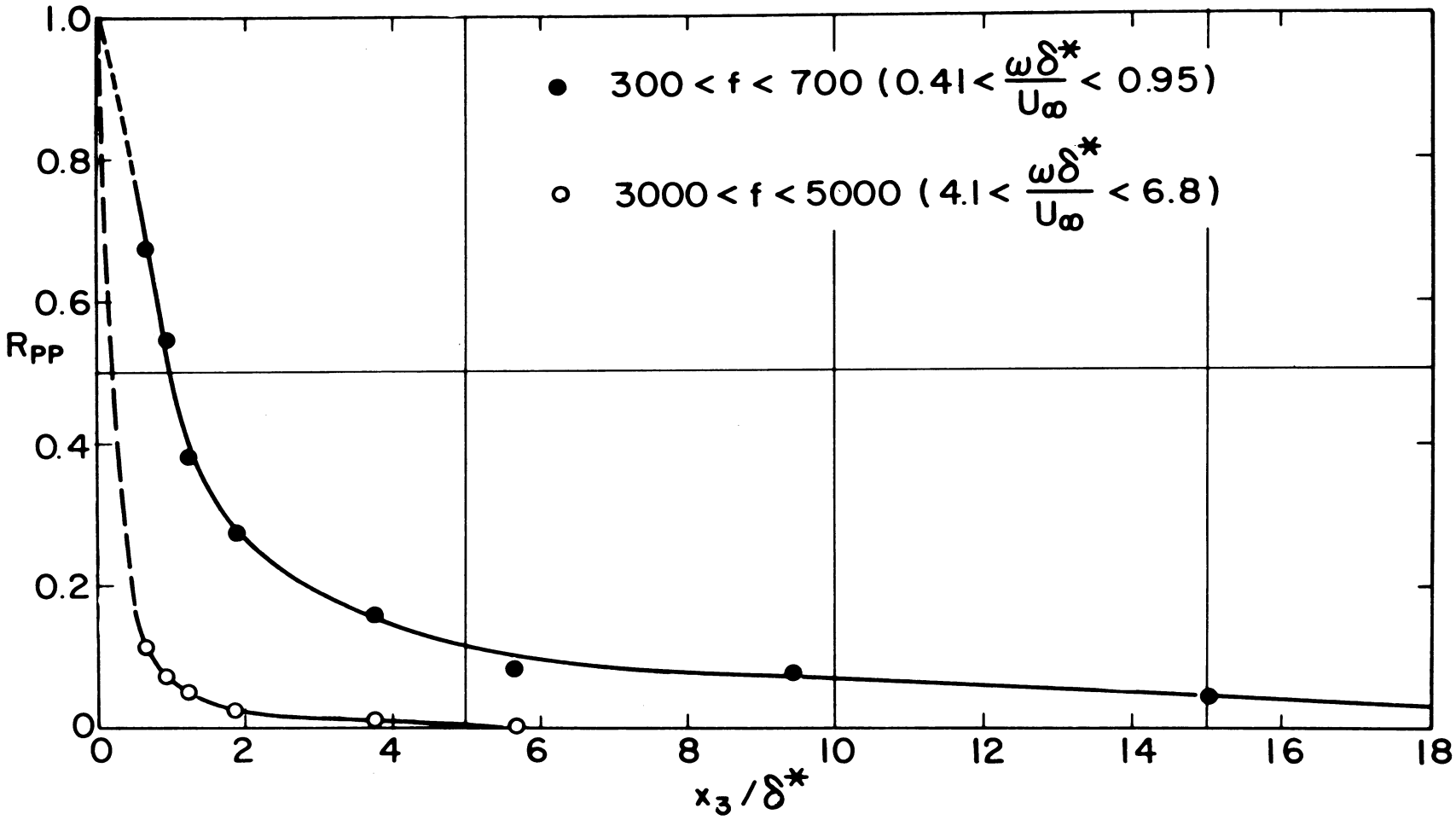

Fig. 12. Transverse wall pressure correlations measured in a low- and a high-frequency band.

DISTRIBUTION LIST
(One copy unless otherwise noted)

Chief of Naval Research
Department of the Navy
Washington 25, D. C.
Attn: Code 438 3
Attn: Code 461
Attn: Code 463
Attn: Code 466

Commanding Officer
Office of Naval Research
Branch Office
495 Summer Street
Boston 10, Massachusetts

Commanding Officer
Office of Naval Research
Branch Office
346 Broadway
New York 13, New York

Commanding Officer
Office of Naval Research
Branch Office
1030 East Green Street
Pasadena, California

Commanding Officer
Office of Naval Research
Branch Office
1000 Geary Street
San Francisco 9, California

Commanding Officer 10
Office of Naval Research
Branch Office
Navy No. 100, Fleet Post Office
New York, New York

Director 6
Naval Research Laboratory
Washington 25, D. C.
Attn: Code 2027

Chief, Bureau of Naval Weapons
Department of the Navy
Washington 25, D. C.
Attn: Code RUAW-4
Attn: Code RRRE
Attn: Code RAAD
Attn: Code RAAD-222
Attn: Code DIS-42

Chief, Bureau of Ships
Department of the Navy
Washington 25, D. C.
Attn: Code 310
Attn: Code 312
Attn: Code 335
Attn: Code 420
Attn: Code 421
Attn: Code 440
Attn: Code 442
Attn: Code 449

Chief, Bureau of Yards and Docks
Department of the Navy
Washington 25, D. C.
Attn: Code D-400

Commanding Officer and Director
David Taylor Model Basin
Washington 7, D. C.
Attn: Code 108
Attn: Code 142
Attn: Code 500
Attn: Code 513
Attn: Code 520
Attn: Code 526
Attn: Code 526A
Attn: Code 530
Attn: Code 533
Attn: Code 580
Attn: Code 585
Attn: Code 589
Attn: Code 591
Attn: Code 591A
Attn: Code 700

DISTRIBUTION LIST (Continued)

Commander
U. S. Naval Ordnance Test Station
China Lake, California
Attn: Code 753

Commander
U. S. Naval Ordnance Test Station
Pasadena Annex
3202 E. Foothill Blvd.
Pasadena 8, California
Attn: Code P-508

Commander
Planning Department
Portsmouth Naval Shipyard
Portsmouth, New Hampshire

Commander
Planning Department
Boston Naval Shipyard
Boston 29, Massachusetts

Commander
Planning Department
Pearl Harbor Naval Shipyard
Navy No. 128, Fleet Post Office
San Francisco, California

Commander
Planning Department
San Francisco Naval Shipyard
San Francisco 24, California

Commander
Planning Department
Mare Island Naval Shipyard
Vallejo, California

Commander
Planning Department
New York Naval Shipyard
Brooklyn 1, New York

Commander
Planning Department
Puget Sound Naval Shipyard
Bremerton, Washington

Commander
Planning Department
Philadelphia Naval Shipyard
U. S. Naval Base
Philadelphia 12, Pennsylvania

Commander
Planning Department
Norfolk Naval Shipyard
Portsmouth, Virginia

Commander
Planning Department
Charleston Naval Shipyard
U. S. Naval Base
Charleston, South Carolina

Commander
Planning Department
Long Beach Naval Shipyard
Long Beach 2, California

Commander
Planning Department
U. S. Naval Weapons Laboratory
Dahlgren, Virginia

Commander
U. S. Naval Ordnance Laboratory
White Oak, Maryland

Dr. A. V. Hershey
Computation and Exterior
Ballistics Laboratory
U. S. Naval Weapons Laboratory
Dahlgren, Virginia

Superintendent
U. S. Naval Academy
Annapolis, Maryland
Attn: Library

DISTRIBUTION LIST (Continued)

Superintendent
U. S. Naval Postgraduate School
Monterey, California

Commandant
U. S. Coast Guard
1300 E Street, N. W.
Washington, D. C.

Secretary Ship Structure Committee
U. S. Coast Guard Headquarters
1300 E Street, N. W.
Washington, D. C.

Commander
Military Sea Transportation Service
Department of the Navy
Washington 25, D. C.

U. S. Maritime Administration
GAO Building
441 G Street, N. W.
Washington, D. C.
Attn: Division of ship Design
Attn: Division of Research

Superintendent
U. S. Merchant Marine Academy
Kings Point, Long Island, New York
Attn: Capt. L. S. McCready (Dept. of Engineering)

Commanding Officer and Director
U. S. Navy Mine Defense Laboratory
Panama City, Florida

Commanding Officer
NROTC and Naval Administrative Unit
Massachusetts Institute of Technology
Cambridge 39, Massachusetts

U. S. Army Transportation Research and Development Command 2
Fort Eustis, Virginia
Attn: Marine Transport Division

Director of Research
National Aeronautics and Space Administration
1512 H Street, N. W.
Washington 25, D. C.

Director
Langley Research Center
Langley Field Virginia
Attn: Mr. J. B. Parkinson 2
Attn: Mr. I. E. Garrick
Attn: Mr. D. J. Marten

Director Engineering Sciences Division
National Science Foundation
1951 Constitution Avenue, N. W.
Washington 25, D. C.

Director
National Bureau of Standards
Washington 25, D. C.
Attn: Fluid Mechanics Division (Dr. G. B. Schubauer)
Attn: Dr. G. H. Keulegan
Attn: Dr. J. M. Franklin

Armed Services Technical Information Agency 10
Arlington Hall Station
Arlington 12, Virginia

Office of Technical Services
Department of Commerce
Washington 25, D. C.

California Institute of Technology
Pasadena 4, California
Attn: Professor M. S. Plesset
Attn: Professor T. Y. Wu
Attn: Professor A. J. Acosta

University of California
Department of Engineering
Los Angeles 24, California
Attn: Dr. A. Powell

DISTRIBUTION LIST (Continued)

Director
Scripps Institute of Oceanography
University of California
La Jolla, California

Professor M. L. Albertson
Department of Civil Engineering
Colorado A and M College
Fort Collins, Colorado

Professor J. E. Cermak
Department of Civil Engineering
Colorado State University
Fort Collins, Colorado

Professor W. R. Sears
Graduate School of Aeronautical Engr.
Cornell University
Ithaca, New York

State University of Iowa
Iowa Inst. of Hydraulic Research
Iowa City, Iowa
Attn: Dr. H. Rouse
Attn: Dr. L. Landweber

Harvard University
Cambridge 38, Massachusetts
Attn: Professor G. Birkhoff
(Dept. of Mathematics)
Attn: Professor G. F. Carrier
(Dept. of Mathematics)

Massachusetts Institute of Technology
Cambridge 39, Massachusetts
Attn: Department of Naval Architecture and Marine Engineering
Attn: Professor A. T. Ippen

University of Michigan
Ann Arbor, Michigan
Attn: Professor R. B. Couch
(Dept. of Naval Architecture)
Attn: Professor W. W. Willmarth
(Aero. Engrg. Department)
Attn: Professor M. S. Uberoi
(Aero. Engrg. Department)

Dr. L. G. Straub, Director
St. Anthony Falls Hydraulic Lab
University of Minnesota
Minneapolis 14, Minnesota
Attn: Mr. J. N. Wetzel
Attn: Professor B. Silberman

Professor J. J. Foody
Engineering Department
New York State University Maritime College
Fort Schuyler, New York

New York University
Institute of Mathematical Sciences
25 Waverly Place
New York 3, New York
Attn: Professor J. Keller
Attn: Professor J. J. Stoker
Attn: Professor R. Kraichnan

The Johns Hopkins University
Department of Mechanical Engineering
Baltimore 18, Maryland
Attn: Professor S. Corrsin
Attn: Professor O. M. Phillips 2

Massachusetts Institute of Technology
Department of Naval Architecture and Marine Engineering
Cambridge 39, Massachusetts
Attn: Prof. M. A. Abkowitz, Head

Dr. G. F. Wislicenus
Ordnance Research Laboratory
Pennsylvania State University
University Park, Pennsylvania
Attn: Dr. M. Sevik

Professor R. C. DiPrima
Department of Mathematics
Rensselaer Polytechnic Institute
Troy, New York

DISTRIBUTION LIST (Continued)

Stevens Institute of Technology
Davidson Laboratory
Castle Point Station
Hoboken, New Jersey
Attn: Professor E. V. Lewis
Attn: Mr. D. Savitsky
Attn: Mr. J. P. Breslin
Attn: Mr. C. J. Henry
Attn: Mr. S. Tsakonas

Webb Institute of Naval Architecture
Crescent Beach Road
Glen Cove, New York
Attn: Technical Library

Director
Woods Hole Oceanographic Institute
Woods Hole, Massachusetts

Commander
Air Research and Development Command
Air Force Office of Scientific Research
14th and Constitution
Washington 25, D. C.
Attn: Mechanics Branch

Commander
Wright Air Development Division
Aircraft Laboratory
Wright-Patterson Air Force Base, Ohio
Attn: Mr. W. Mykytow, Dynamics Branch

Cornell Aeronautical Laboratory
4455 Genesee Street
Buffalo, New York
Attn: Mr. W. Targoff
Attn: Mr. R. White

Massachusetts Institute of Technology
Fluid Dynamics Research Laboratory
Cambridge 39, Massachusetts
Attn: Professor H. Ashley
Attn: Professor M. Landahl
Attn: Professor J. Dugundji

Hamburgische Schiffbau-Versuchsanstalt
Bramfelder Strasse 164
Hamburg 33, Germany
Attn: Dr. O. Grim
Attn: Dr. H. W. Lerbs

Institut für Schiffbau der
Universität Hamburg
Berliner Tor 21
Hamburg 1, Germany
Attn: Professor G. P. Weinblum, Director

Max-Planck Institut für Strömungsforschung
Bottingerstrasse 6/8
Gottingen, Germany
Attn: Dr. H. Reichardt

Hydro-og Aerodynamisk Laboratorium
Lyngby, Denmark
Attn: Professor Carl Prohaska

Skipsmodelltanken
Trondheim, Norway
Attn: Professor J. K. Lunde

Versuchsanstalt für Wasserbau und Schiffbau
Schleuseninsel im Tiergarten
Berlin, Germany
Attn: Dr. S. Schuster, Director

Technische Hogeschool
Institut voor Toegepaste Wiskunde
Julianalaan 132
Delft, Netherlands
Attn: Professor R. Timman

Bureau D'Analyse et de Techerche
Appliquees
47 Avenue Victor Cresson
Issy les Moulineaux (Seine)
Paris, France
Attn: Professor Siestrunck

Netherlands Ship Model Basin
Wageningen, Netherlands
Attn: Dr. Ir. J. D. van Manen

National Physical Laboratory
Teddington, Middlesex, England
Attn: Dr. F. H. Todd, Superintendent
Ship Division
Attn: Head Aerodynamics Division
Attn: Mr. A. Silverleaf

Head, Aerodynamics Department 2
Royal Aircraft Establishment
Farnborough, Hants, England
Attn: Mr. M. O. W. Wolfe

Boeing Airplane Co.
Seattle Division
Seattle, Washington
Attn: Mr. M. J. Turner

Electric Boat Division
General Dynamics Corporation
Groton, Connecticut
Attn: Mr. Robert McCandliss

General Applied Sciences Labs, Inc.
Merrick and Stewart Avenues
Westbury, Long Island, New York

Gibbs and Cox, Inc.
21 West Street
New York, New York

Grumman Aircraft Engineering Corp.
Bethpage, Long Island, New York
Attn: Mr. E. Baird
Attn: Mr. E. Bower

Grumman Aircraft Engineering Corp.
Dynamic Developments Division
Babylon, New York

Lockheed Aircraft Corporation
Missiles and Space Division
Palo Alto, California
Attn: R. W. Kermeen

Midwest Research Institute
425 Volker Blvd.
Kansas City 10, Missouri
Attn: Mr. Zeydel

Director, Department of Mechanical
Sciences
Southwest Research Institute
8500 Culebra Road
San Antonio 6, Texas
Attn: Dr. H. N. Abramson
Attn: Mr. G. Ransleben
Attn: Editor, Applied Mechanics
Review

Convair
A Division of General Dynamics
San Diego, California
Attn: Mr. R. H. Oversmith
Attn: Mr. A. D. MacLellan
Attn: Mr. H. T. Brooke

Dynamic Developments, Inc.
15 Berry Hill Road
Oyster Bay, Long Island, New York

Dr. S. F. Hoerner
148 Busteed Drive
Midland Park, New Jersey

Hydronautics, Incorporated
200 Monroe Street
Rockville, Maryland
Attn: Mr. Phillip Eisenberg

DISTRIBUTION LIST (Concluded)

Rand Development Corporation
13600 Deise Avenue
Cleveland 10, Ohio
Attn: Dr. A. S. Iberall

U. S. Rubber Company
Research and Development Department
Wayne, New Jersey
Attn: Mr. L. M. White

Technical Research Group, Inc.
2 Aerial Way
Syosset, Long Island, New York
Attn: Mr. Jack Kotik
Attn: Dr. Sheldon Gardner